The effect of leading-edge droop on the performance of cavitating hydrofoil in an oscillating environment

K Park[1], **H Sun**[2], and **S Lee**[3]*

[1]School of Mechanical and Aerospace Engineering, Seoul National University, Sillim-dong, Gwanak-gu, Seoul, Republic of Korea

[2]Korea Environment Institute, Jinheungno, Eunpyeong-Gu, Seoul, Republic of Korea

[3]Institute of Advanced Aerospace Technology, School of Mechanical and Aerospace Engineering, Seoul National University, Sillim-dong, Gwanak-gu, Seoul, Republic of Korea

The manuscript was received on 15 April 2008 and was accepted after revision for publication on 28 April 2009.

DOI: 10.1243/09544062JMES1142

Abstract: The hydrodynamics of cavitating hydrofoil in oscillating motion are important in the aspect of the performance and hydro-elasticity of the control surface of the ship. The effect of leading-edge droop is numerically studied in the oscillating hydrofoil with cavitation. A two-phase incompressible Navier–Stokes solver is used to compute the cavitation flow. The hydrodynamic performance of the baseline hydrofoil is compared with that of the fixed droop and the variable droop hydrofoil. The droop models delay the separation behind the sheet cavitation near the maximum angle of attack. When the pitch goes down, the drooped models suppress the collapse of the sheet cavitation. Therefore, they result in the improved hydrodynamic performance against the baseline model through the oscillation cycle. Among the three hydrofoils, the variable droop showed the smallest change of the lift-to-drag ratio.

Keywords: cavitation, leading-edge droop, hydrofoil, performance

1 INTRODUCTION

Cavitation leads to a decrease in hydrodynamic performance and efficiency and also causes erosion on the fluid machinery. In the field of ship building, the cavitation on hydrofoils becomes more important as the speed of ships increases. The hydrofoils are used as stabilizers and control surfaces in the ship and submarine. Using hydrofoil under cavitation conditions, the steering force reduces because of a decrease in suction pressure, and the erosion on the surface accelerates. These adverse effects result in an increase in control difficulty and cost of maintenance. For over 50 years, researchers have studied cavitating hydrofoils to examine characteristics of the cavitation flow and acoustics and to develop designs that reduce cavitation on stationary hydrofoil.

Hydrofoils may experience not only stationary motion but also oscillating motion because of manoeuvring or hydro-elasticity in many practical cases. Cavitating hydrofoil in oscillating motion has mainly been studied in the aspect of flow. Hart *et al.* [**1**] found that cavitation formation and inception are dependent on reduced hydrofoil frequency. Oscillating hydrofoil with cavitation was simulated through computational fluid dynamics by Kinzel *et al.* [**2**], and solved using Navier–Stokes equation with liquid–vapour mass-transfer model and overset grid technique.

These researches focused on the cavitation phenomenon itself or the prediction method of the oscillating hydrofoil. Other studies involve methods to improve the performance of the oscillating hydrofoil with cavitation. Similarly, this study suggests a design concept to improve the hydrodynamic performance using leading-edge droop. The leading-edge droop concept was developed for dynamic stall control in the field of helicopters. The design is obtained by drooping the forward portion of the aerofoil at a high angle of attack. It makes the flow pass smoothly without the separation on the upper surface of the

*Corresponding author: School of Mechanical and Aerospace, Seoul National University, San56-1, Sillim-dong, Gwanak-gu, Seoul 151-742, Republic of Korea.
email: solee@snu.ac.kr

aerofoil. Lee *et al.* [**3**] and Geissler and Trenker [**4**] employed a variable leading-edge droop aerofoil for dynamic stall control and showed how it improved the characteristics of the pitching moment.

In this study, cavitation flow of the oscillating hydrofoil is numerically analysed using a two-phase Navier–Stokes solver. The leading-edge droop hydrofoils, fixed droop and variable droop, are compared with baseline hydrofoil, and the effects are studied in the aspect of hydrodynamic performance.

2 FLOW SOLVER

2.1 Numerical method

The governing equations for cavitating flow analysis are Navier–Stokes equations with a volume fraction transport equation and are as follows [**5**]

$$\begin{aligned}
&\left(\frac{1}{\rho_m \beta}\right)\frac{\partial p}{\partial \tau} + \frac{\partial u_j}{\partial x_j} = (\dot{m}^+ \dot{m}^-)\left(\frac{1}{\rho_l} - \frac{1}{\rho_v}\right)\\
&\frac{\partial}{\partial t}(\rho_m u_i) + \frac{\partial}{\partial \tau}(\rho_m u_i) + \frac{\partial}{\partial x_j}(\rho_m u_i u_j) = \frac{\partial p}{\partial x_j} + \frac{\partial \hat{\tau}_{ij}}{\partial x_j}\\
&\frac{\partial \alpha_l}{\partial t} + \left(\frac{\alpha_i}{\rho_m \beta}\right)\frac{\partial p}{\partial \tau} + \frac{\partial \alpha_l}{\partial \tau} + \frac{\partial}{\partial x_j}(\alpha_i u_j)\\
&\quad = (\hat{m}^+ + \hat{m}^-)\left(\frac{1}{\rho_l}\right)
\end{aligned} \tag{1}$$

where ρ_m is the gas–liquid mixture density defined by

$$\rho_m = \rho_l \alpha_l + \rho_v (1 - \alpha_l) \tag{2}$$

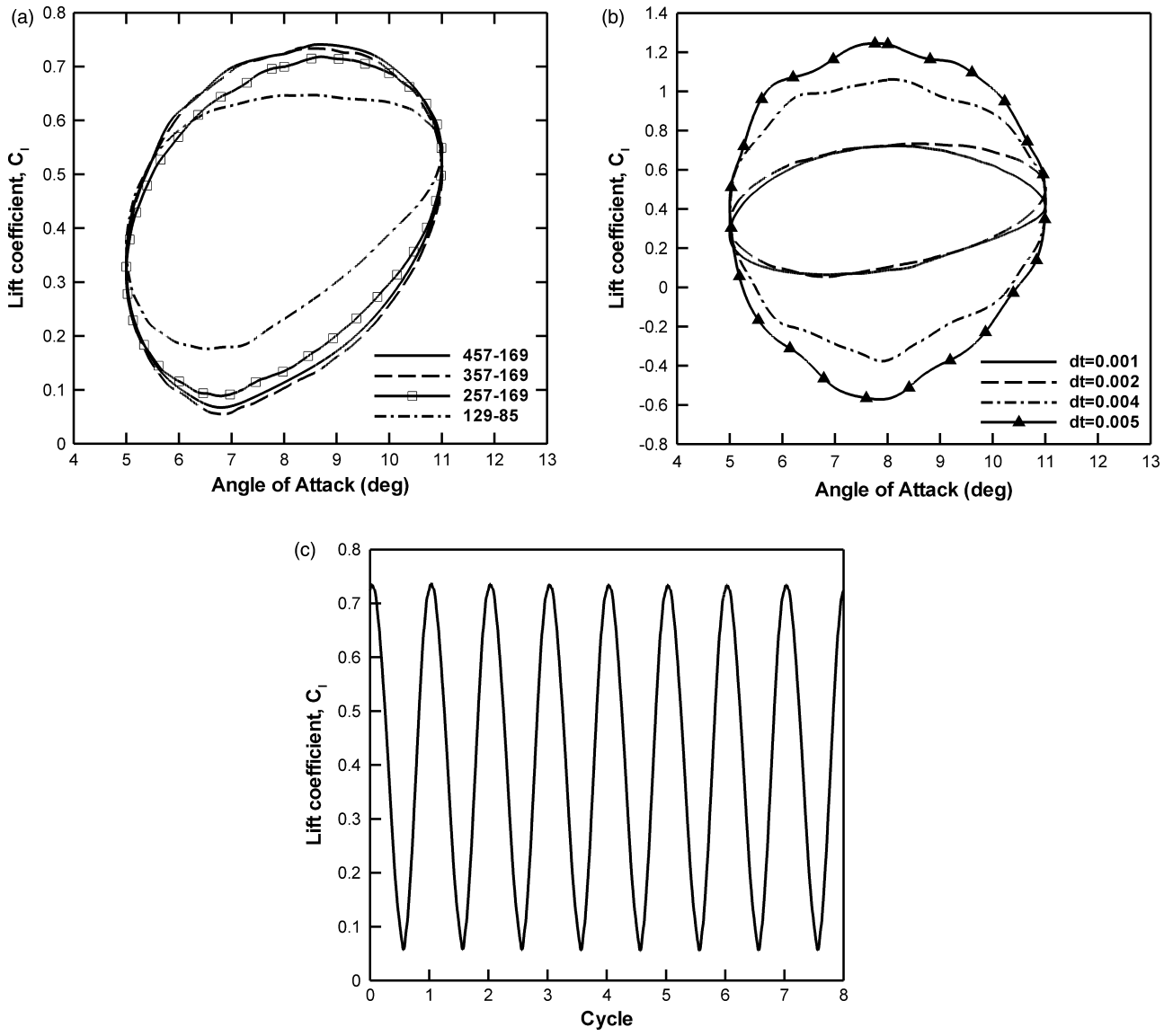

Fig. 1 Effects of grid size and time step and the history of the lift coefficient: (a) mesh size sensitivity; (b) time-step influence; and (c) convergence to periodic solution

In equation (1), τ is the pseudo-time, t is the physical time, β is the pseudo-compressibility parameter (here, it is 800), x_j are the Cartesian coordinates, u_j are the Cartesian components of the velocity, p is the static pressure, and $\hat{\tau}_{ij}$ is composed of molecular and Reynolds stresses expressed as

$$\hat{\tau}_{ij} = 2\mu_{m,\mathrm{l}}\left(\frac{S_{ij} - S_{kk}\delta_{ij}}{3}\right) + \tau_{ij}$$

$$\tau_{ij} = 2\mu_{m,\mathrm{t}}\left(\frac{S_{ij} - S_{kk}\delta_{ij}}{3}\right) - \frac{2\rho_m k\delta_{ij}}{3}$$

$$S_{ij} = \frac{1}{2}\left(\frac{\partial u_i}{\partial x_j} + \frac{\partial u_j}{\partial x_i}\right) \tag{3}$$

In order to consider the phase change, the mass transfer rates, $\dot{m}^+$ and $\dot{m}^-$, are introduced as the source terms of the Navier–Stokes equation. $\dot{m}^+$ and $\dot{m}^-$ denote mass transfer rate from the vapour to the liquid and mass transfer rate from the liquid to the vapour, respectively. A simplified form of the Ginzburg–Landau potential is employed in $\dot{m}^+$, and $\dot{m}^-$ is modelled as being proportional to the liquid volume fraction and the amount by difference of static

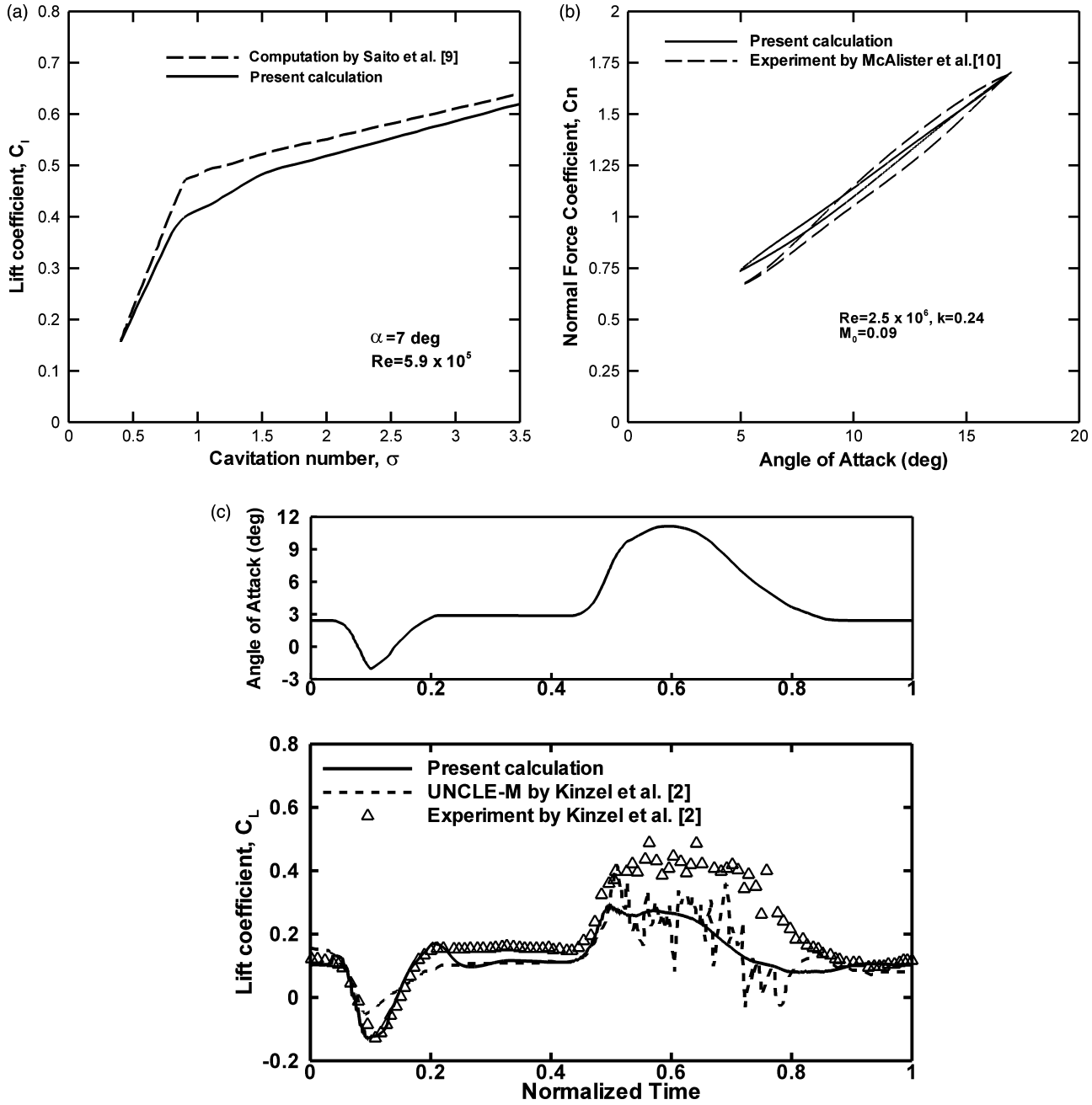

Fig. 2 Validation results: (a) stationary hydrofoil; (b) oscillating hydrofoil in the non-cavitation condition; and (c) oscillating hydrofoil in the cavitation condition

pressure and vapour pressure [**5**]

$$\dot{m}^- = \frac{C_{\text{dest}}\rho_v\alpha_l \min[0, p - p_v]}{(1/2\rho_l u_\infty^2)t_\infty}$$
$$\dot{m}^+ = \frac{C_{\text{prod}}\rho_v\alpha_l^2(1-\alpha_l)}{t_\infty} \tag{4}$$

where C_{dest} and C_{prod} are the empirical constants (here, $C_{\text{dest}} = 100$ and $C_{\text{prod}} = 100$).

In this study, the transformed k–ε turbulence model is adopted to take the turbulence effect into account [**6**]. The model has the transport equations for the turbulent kinetic energy k and the specific turbulent dissipation rate ε and is expressed as

$$\frac{\partial \rho_m k}{\partial t} + \frac{\partial}{\partial x_j}(\rho_m k u_j) = \tau_{ij}\frac{\partial u_i}{\partial x_j} - \beta^*\rho_m\omega k + \frac{\partial}{\partial x_j}\left[(\mu_{m,l} + \sigma_k\mu_{m,t})\frac{\partial k}{\partial x_j}\right]$$
$$\frac{\partial \rho_m \omega}{\partial t} + \frac{\partial}{\partial x_j}\left(\rho_m\omega u_j\right) = \frac{\gamma}{\nu_{m,t}}\tau_{ij}\frac{\partial u_i}{\partial x_j} - \beta\rho_m\omega^2 + \frac{\partial}{\partial x_j}\left[(\mu_{m,l} + \sigma_\omega\mu_{m,t})\frac{\partial \omega}{\partial x_j}\right] + 2\rho_m\sigma_\omega\frac{1}{\omega}\frac{\partial k}{\partial x_j}\frac{\partial \omega}{\partial x_j} \tag{5}$$

where $\nu_{m,t}$ is the turbulent mixture kinematic viscosity.

The governing equation is solved by using an implicit finite-volume method. For the calculation of the residual, the convective terms are discretized using the third-order upwind differencing scheme with monotone upstream centered scheme for conservation law (MUSCL) approach [**7**], and the viscous terms are differenced using second-order central difference. Lower-upper symmetric Gauss-Seidel (LU-SGS) scheme is applied for temporal integration of the governing equation [**8**].

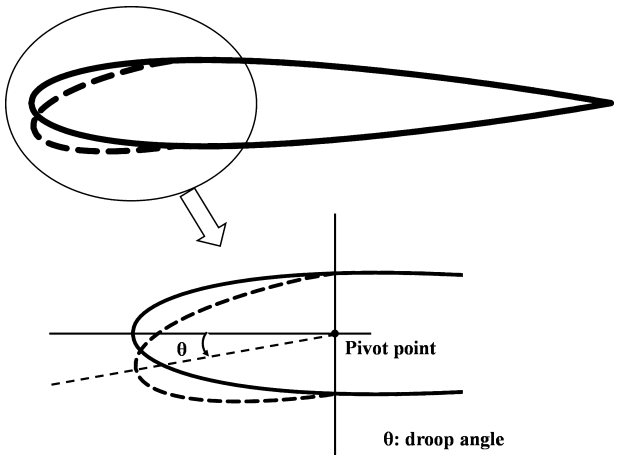

Fig. 3 Schematic of leading-edge droop hydrofoil

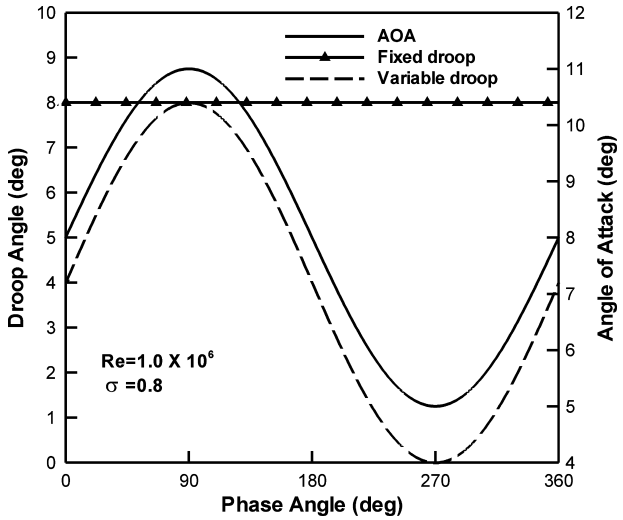

Fig. 4 Angle of attack and change of the droop angle during one cycle

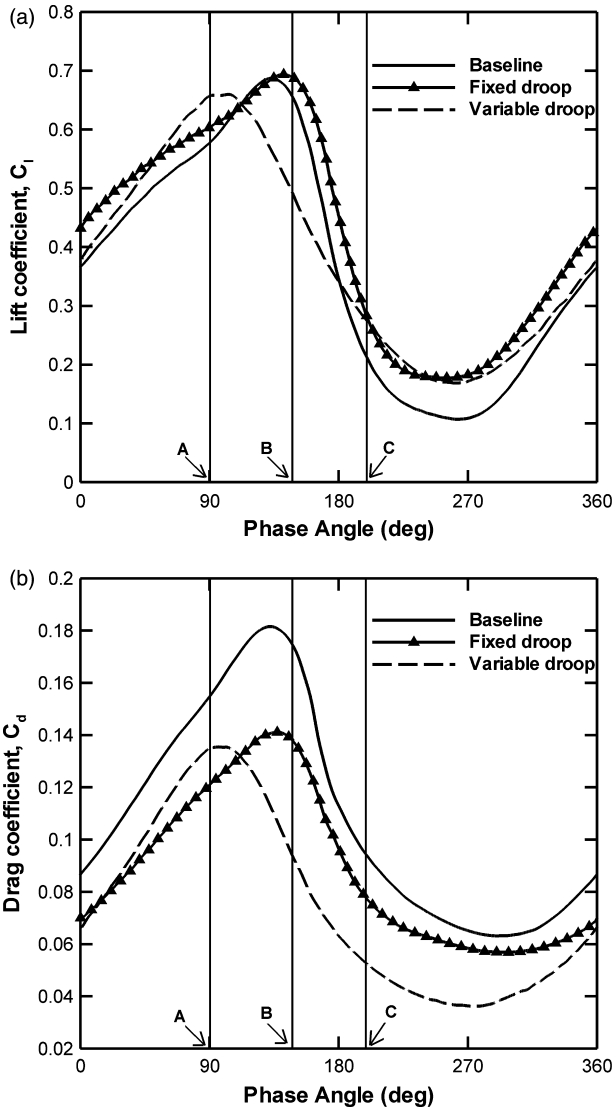

Fig. 5 Hydrodynamic coefficients of three hydrofoils: (a) lift coefficient and (b) drag coefficient

2.2 Validations

The mesh size sensitivity, time-step influence, and convergence to periodic solution were investigated in the cavitation flow over an oscillating NACA 0015 hydrofoil. The studies were computed at the Reynolds number of 1.0×10^6, the cavitation number of 1.0, the mean angle of attack α_0 of 8°, the amplitude of angle of attack α_m of 3°, and the reduced frequency k of 1.0. The angle of attack α of sinusoidal oscillating hydrofoil varies as follows

$$\alpha = \alpha_0 + \alpha_m \sin(2kt) \tag{6}$$

The mesh size sensitivity was studied with the O-type grid system, in which the grid sizes were 129×85, 257×169, 357×169, and 457×169 in the streamwise and the normal directions, respectively. As Fig. 1(a) shows that the difference of the lift coefficient between 457×169 and 357×169 grids is small, the grid with the size of 357×169 is chosen to simulate the oscillating hydrofoil. The time-step size influence was examined through the time steps of 0.001, 0.002, 0.004, and 0.005 (Fig. 1(b)). Although there is small difference between 0.001 and 0.002, simulations are implemented at the time step of 0.002 in order to reduce computational cost. Figure 1(c) displays the periodic change of the lift coefficient after convergence.

A stationary hydrofoil in cavitation condition and the oscillating hydrofoils in non-cavitation and cavitation conditions were simulated to validate. The calculation of the stationary cavitating hydrofoil was validated by comparing with Saito *et al.*'s prediction [**9**]. It was carried out on the CAV2003 hydrofoil at an angle of attack of 7° and Reynolds number of 5.9×10^5.

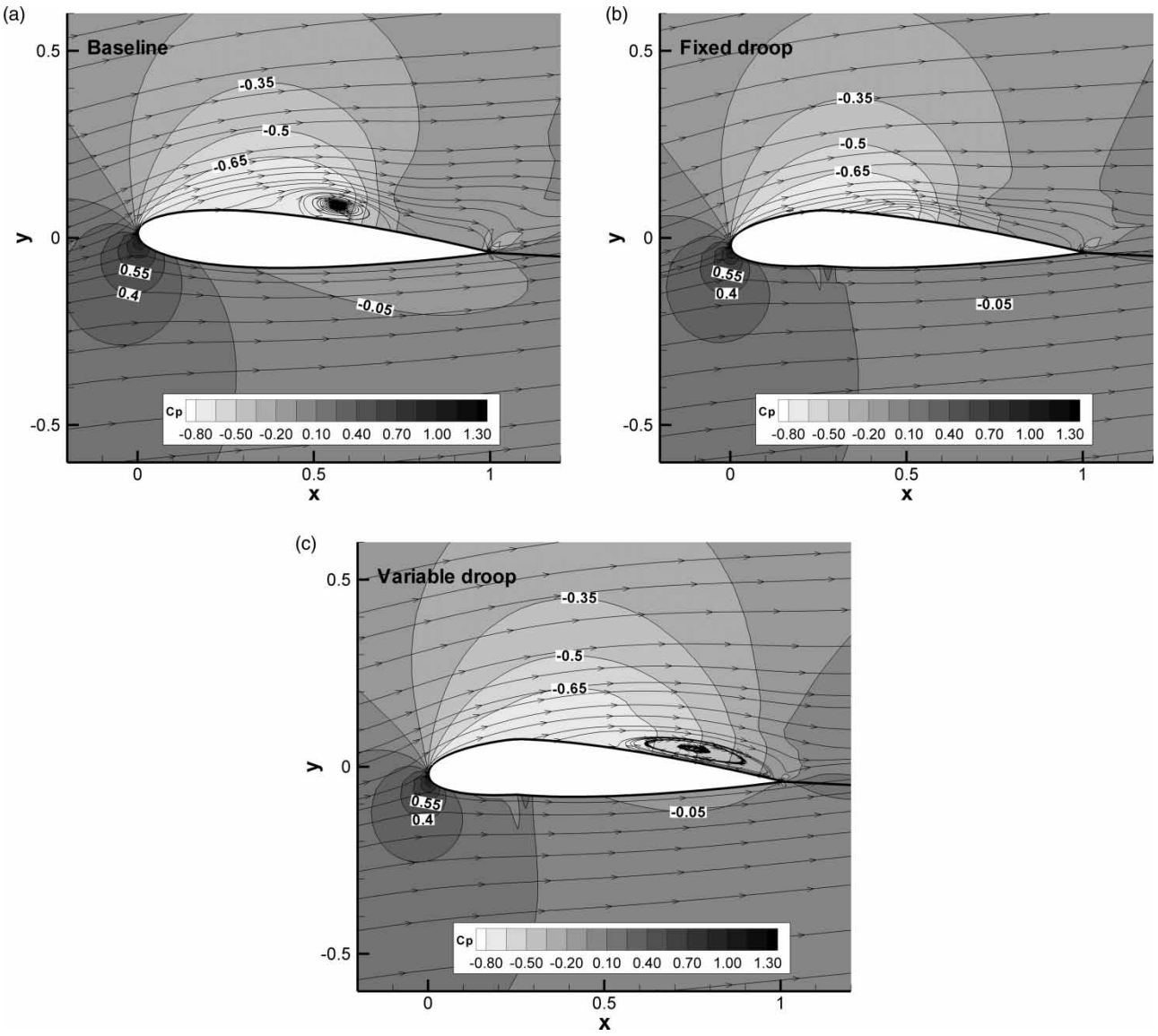

Fig. 6 Streamlines and pressure contours of three hydrofoils at $\alpha = 11°$: (a) baseline; (b) fixed droop; and (c) variable droop

As shown in Fig. 2(a), the similar performance curve between two predictions is observed.

For the validation of the oscillating hydrofoil without the cavitation, the prediction result was compared with the experimental one by McAlister *et al.* [**10**]. The flow parameters for the simulation were as follows: the mean angle of attack of 11°, the amplitude of angle of attack of 6°, the Reynolds number of 2.5×10^6, and the reduced frequency of 0.24. The computation yields reasonable agreement with the experiment as in Fig. 2(b). In order to validate the oscillating hydrofoil with cavitation, the calculation was compared with Kinzel *et al.*'s study [**2**]. It is performed at Reynolds number of 5.0×10^5, reduced frequency of 0.05, and cavitation number of 0.6. The angle of attack changes from −2° to 11° as in Fig. 2(c). When the calculation is compared to the experiment, there is some difference of the lift coefficient after the normalized time, 0.5. However, the lift in minus angle of attack shows good agreement with the experiment. Compared to UNCLE-M, the performance of the prediction is reasonable. As shown in Fig. 2, the calculated results show reasonable agreement to compare the relative performances by leading-edge droop and suggest the design concept.

3 RESULTS AND DISCUSSION

NACA0015 hydrofoil was used to simulate oscillating hydrofoil and to investigate the change of the performance and the cavitation by using leading-edge droop. Figure 3 displays the schematic of the leading-edge droop hydrofoil. The drooped hydrofoil is obtained by rotating the forepart of the baseline hydrofoil about a pivot point. The quarter chord point from the leading edge was the pivot point for the drooping and the

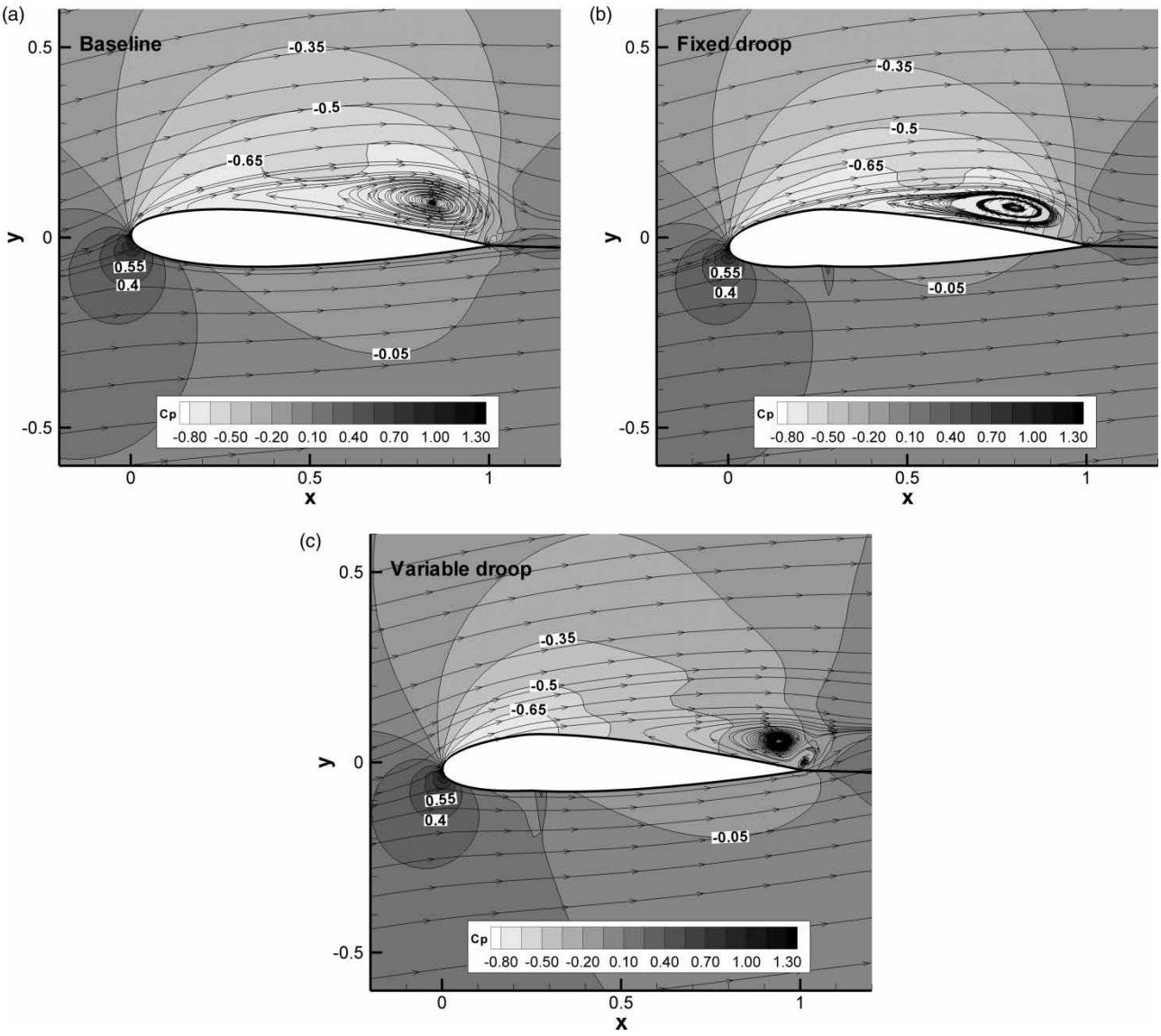

Fig. 7 Streamlines and pressure contours of three hydrofoils at $\alpha = 9.6°$ (downstroke): (a) baseline; (b) fixed droop; and (c) variable droop

oscillating axis of the hydrofoil. The simulation was carried out at Reynolds number of 1.0×10^6, cavitation number of 0.8, and reduced frequency of 0.63. As shown in Fig. 4, the drooped angle of 8° was applied for the fixed and variable droop, and drooping frequency of the variable droop hydrofoil was equal to oscillation reduced frequency.

As the baseline hydrofoil was compared to the fixed droop and variable droop hydrofoil, the effect of leading-edge droop was examined. The lift coefficients and the drag coefficients during one cycle are shown in Fig. 5. The characteristics of the lift and drag are improved by leading-edge droop. It is found that in the aspect of drag coefficient, the variable droop model is superior to others.

Figures 6, 7, and 8 display the pressure contours and streamlines at A, B, and C points in Fig. 5, respectively. At point A with an angle of attack of 11°, the recirculation flow was observed on the upper surface for the baseline and the variable droop. The flow is related to the flow separation behind the closure part of the sheet cavitation. For the baseline hydrofoil, it occurred near the mid chord of the upper surface, and its length was about 0.4c. The recirculation of the variable model was developed at about 0.7c from the leading edge because the flow separation was delayed by drooping. A strong vortex attached to the surface leads to suction force, but in the cavitation flow, the minimum pressure due to the attached vortex is restricted to the vapour pressure. As the vortex on the upper surface of the variable droop occurred at the rear of the upper surface against baseline, the lift coefficient of the variable droop was higher than that of the baseline.

At point B with an angle of attack of 9.6°, the hydrofoils were under the downstroke motion, and the

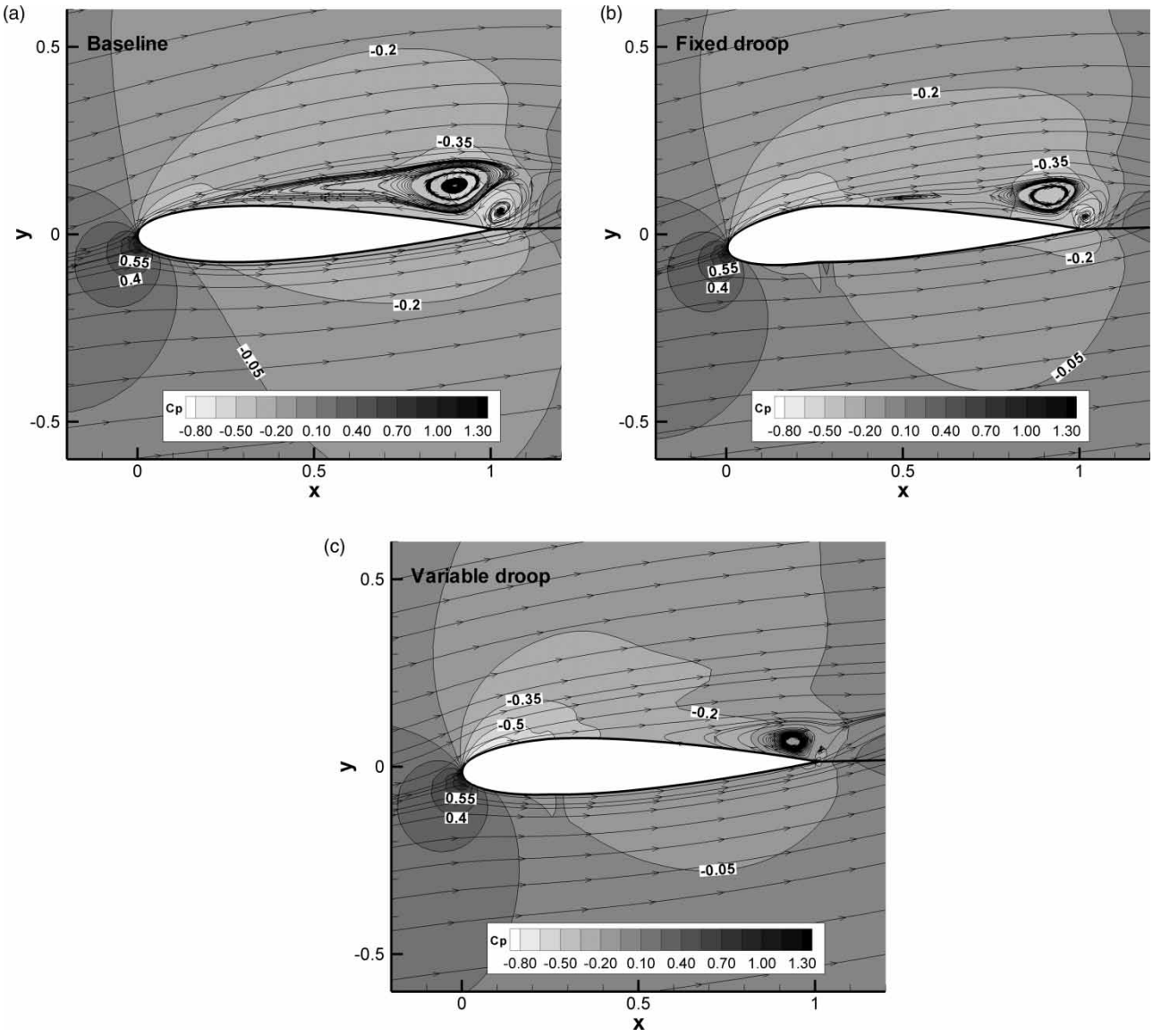

Fig. 8 Streamlines and pressure contours of three hydrofoils at $\alpha = 7.0°$ (downstroke): (a) baseline; (b) fixed droop; and (c) variable droop

large vortex was developed for all cases (Fig. 7). The vortex, which had occurred at about the maximum angle of attack, was convected downstream. The vortex flows of the baseline and the fixed droop hydrofoil act like a dynamic stall vortex in the non-cavitation flow. They led to the increase of the lift coefficient after the maximum angle of attack. Although the lift was increased by reducing the surface pressure to the vapour pressure at the rear part, the pressure reduction resulted in an increase of drag. In the case of the variable droop, the vortex near the trailing edge was weakened after the maximum angle of attack and split into two vortices.

When the hydrofoil was pitching down towards the minimum angle of attack, the large vortex was slightly detached from the upper surface in the case of the baseline and the fixed droop (point C with an angle of attack of 7° in Figs 5 and 8). With pitch down, the sheet cavitation collapses, and the recirculation flow proceeds to the nose part of the hydrofoil. For the baseline, the reverse flow because of recirculation got to about 0.1c position from the leading edge. The collapse of the sheet cavitation brought the increase of the surface pressure above the vapour pressure. Therefore, the increased pressure at the nose led to low lift and high drag. On the other hand, the drooped hydrofoil suppressed the collapse of the cavitation during downstroke and maintained the hydrodynamic performance better than baseline.

Because it is known that oscillating aerofoil in the air has different flow characteristics according to the reduced frequency, the lift-to-drag ratio was calculated to observe the effect of leading-edge droop at the reduced frequencies of 0.25, 0.63, and 1.0. Figure 9 shows the lift-to-drag ratio of the baseline and the drooped hydrofoils with respect to the oscillating

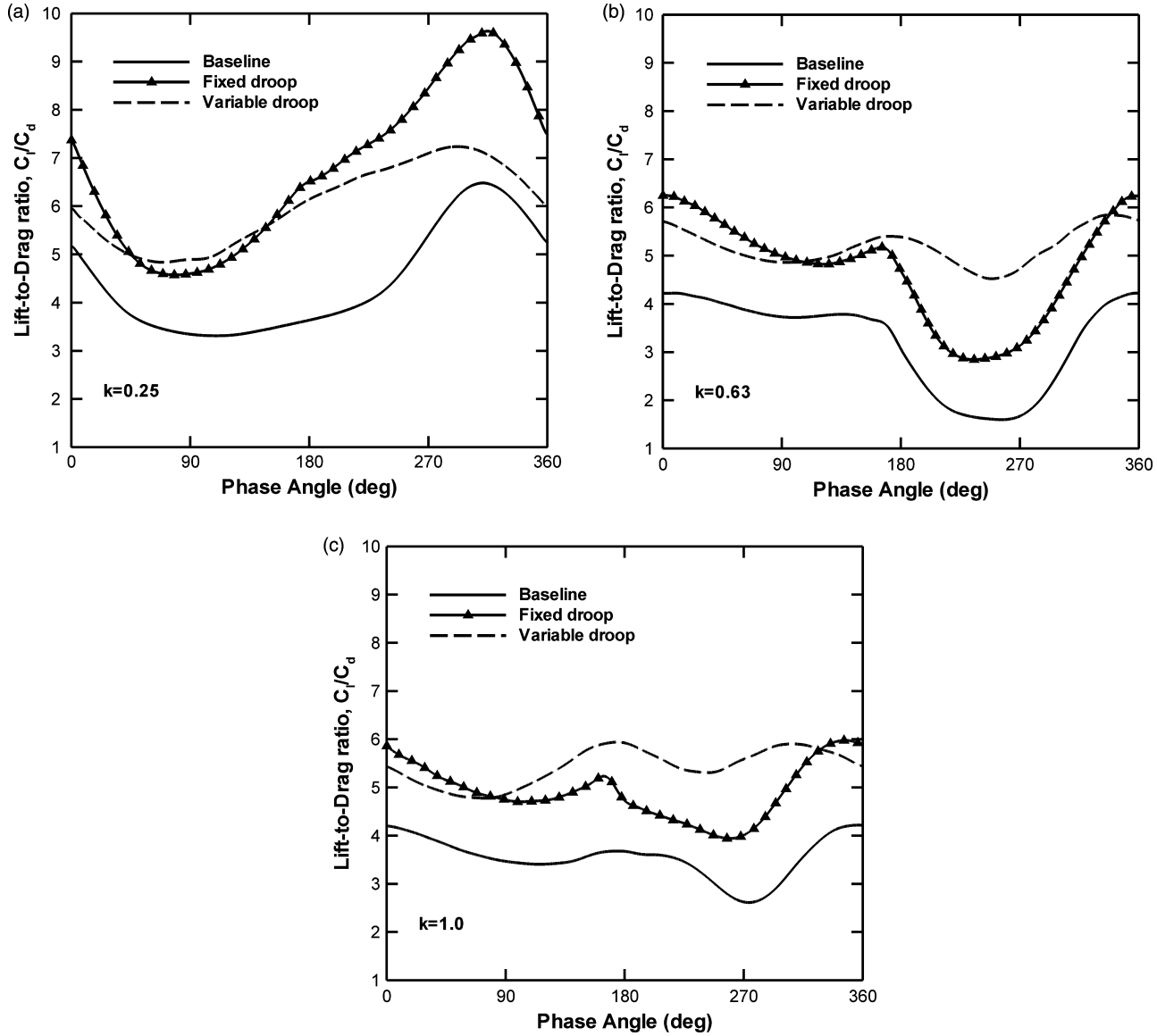

Fig. 9 Lift-to-drag ratio during one cycle according to reduced frequency: (a) $k = 0.25$; (b) $k = 0.63$; and (c) $k = 1.0$

phase angle, using the flow conditions as in Fig. 4. The ratio of the drooped hydrofoil is higher than that of the baseline through the whole phase angle. In the flow with reduced frequencies of 0.63 and 1.0, the performance of the variable droop was higher than that of the fixed droop, but in reduced frequency of 0.25, the fixed droop was better than the variable droop. For the three reduced frequencies, the variable droop showed the smallest change of the lift-to-drag ratio through the cycle. In this study, it was found that application of leading-edge droop could improve the hydrodynamic performance in oscillating hydrofoil with cavitation.

4 CONCLUSIONS

The effect of leading-edge droop was numerically studied in oscillating hydrofoil with the cavitation. A two-phase incompressible Navier–Stokes solver was used to simulate the cavitating hydrofoils. The leading-edge droop hydrofoils, fixed droop and variable droop, were compared with a baseline hydrofoil, NACA0015. The drooped hydrofoil showed improved hydrodynamic performance against the baseline model. Recirculation flow occurred near the maximum angle of attack, and its length and convection had great influence on the performance. A large vortex with recirculation flow led to the increase of lift for the baseline and drooped hydrofoils around the maximum angle of attack. With pitch down, the sheet cavitation of the baseline collapsed rapidly, and the recirculation flow proceeds to the nose part of the hydrofoil. On the other hand, by using droop hydrofoil, collapse of the cavitation was suppressed and the hydrodynamic performance was improved. It was found that compared to variable droop, the fixed droop resulted in higher change of the lift-to-drag ratio. Further study on the optimization of the droop angle is needed to practically apply to the cavitating stabilizer of the ship.

ACKNOWLEDGEMENTS

This work is the outcome of a Manpower Development Program for Energy & Resources supported by the Ministry of Knowledge and Economy (MKE) in Korea. This study was also supported by Engineering Research Institute in Seoul National University.

REFERENCES

1 **Hart, D. P., Brennen, C. E.,** and **Acosta, A. J.** Observations of cavitation on a three-dimensional oscillating hydrofoil. FED-98, 1990, pp. 49–52.

2 **Kinzel, M. P., Willits, S. M., Lindau, J. W., Boger, D. A., Kunz, R. F.,** and **Medvitz, R. B.** CFD simulations of oscillating hydrofoils with cavitation. In Proceedings of the 44th AIAA Aerospace Sciences Meeting and Exhibit, Reno, Nevada, 2006, AIAA paper 2006-1279.

3 **Lee, S., McAlister, K.,** and **Tung, C.** Characteristics of deformable leading edge for high performance rotor. In Proceedings of the AIAA 11th Applied Aerodynamics Conference, CA, USA, 1993.

4 **Geissler, W.** and **Trenker, M. T.** Numerical investigation of dynamic stall control by a nose-drooping device. In Proceedings of the Aerodynamics, Acoustics and Test and Evaluation Technical Specialist Meeting, San Francisco, CA, January 2002 (American Helicopter Society).

5 **Kunz, R. F., Boger, D. A., Stinebring, D. R., Chyczewski, T. S., Lindau, J. W., Gibeling, H. J., Venkateswaran, S.,** and **Govindan, T. R.** A preconditioned Navier–Stokes method for two-phase flows with applications to cavitation prediction. *Comput. Fluids*, 2000, **29**, 849–875.

6 **Menter, F. R.** and **Rumsey, L. C.** Assessment of two-equation turbulence models for transonic flows. AIAA paper 94-2343, 1994.

7 **Sweby, P. K.** High resolution TVD schemes using flux limiters. *Lect. Appl. Math.*, 1985, **22**, 289–309.

8 **Jameson, A.** and **Yoon, S.** Lower–upper implicit schemes with multiple grids for the Euler equations. *AIAA J.*, 1987, **25**, 929–935.

9 **Saito, Y., Nakamori, I.,** and **Ikohagi, T.** Numerical analysis of unsteady vaporous cavitating flow around a hydrofoil. In Proceedings of the Fifth International Symposium on *Cavitation*, Osaka, Japan, 2003.

10 **McAlister, K. W., Carr, L. W.,** and **McCrosky, W. J.** Dynamic stall experiments on the NACA0012 airfoil. NASA technical paper 1100, 1978.

APPENDIX

Notation

c	chord length
c_{d}	two-dimensional drag coefficient
c_{l}	two-dimensional lift coefficient
$c_{\mathrm{l}}/c_{\mathrm{d}}$	lift-to-drag ratio
c_{n}	normal force coefficient
C_{L}	three-dimensional lift coefficient
k	reduced frequency, $\omega c/2U_\infty$
t	physical time
M_0	freestream Mach number
Re	Reynolds number
U_∞	freestream velocity
α	angle of attack
α_0	mean angle of attack
α_m	amplitude of angle of attack
θ	droop angle
σ	cavitation number
ω	angular velocity